UCLA
UCLA Previously Published Works

Title

Polyrotaxane Nanocarriers Can Deliver CRISPR/Cas9 Plasmid to Dystrophic Muscle Cells to Successfully Edit the DMD Gene

Permalink

https://escholarship.org/uc/item/4pp0q6pq

Journal

Advanced Therapeutics, 2(7)

ISSN

2366-3987

Authors

Emami, Michael R
Young, Courtney S
Ji, Ying
et al.

Publication Date

2019-07-01

DOI

10.1002/adtp.201900061

Peer reviewed

Polyrotaxane Nanocarriers Can Deliver CRISPR/Cas9 Plasmid to Dystrophic Muscle Cells to Successfully Edit the DMD Gene

Michael R. Emami, Courtney S. Young, Ying Ji, Xiangsheng Liu, Ekaterina Mokhonova, April D. Pyle,* Huan Meng,* and Melissa J. Spencer*

Gene editing with clustered regularly interspaced short palindromic repeats and CRISPR-associated protein 9 (CRISPR/Cas9) has shown promise in models of Duchenne muscular dystrophy (DMD); however, nonviral strategies to deliver CRISPR to muscle have not been widely explored or optimized. Most studies have relied on viral vectors, which are likely limited to single dosing due to their immunogenicity, thus reducing their therapeutic potential. Therefore, there is a need to develop nonviral approaches that allow for delivery and repeat dosing of CRISPR/Cas9 therapies to skeletal muscle. Here, biocompatible multi-arm polyrotaxane (PRX) nanocarriers, are iteratively optimized for packaging large plasmid DNA for delivery to muscle cells. The PRXs are optimized by addition of a disulfide-responsive linker that enhances plasmid release. Furthermore, conjugation of peptides leads to quicker uptake and improved transfection efficiency in humanized dystrophic muscle cells in vitro. Finally, in vitro delivery of PRXs complexed with a CRISPR/Cas9 platform demonstrates effective deletion of DMD exons 45–55, a therapeutic strategy with potential to restore the reading frame for half of DMD patients. This work represents the first PRX platform that is optimized and designed for delivery of large plasmid DNA, such as CRISPR/Cas9, to dystrophic muscle cells.

1. Introduction

Gene editing has wide-ranging possibilities for improving human life, such as modifying crop and livestock genomes, creating novel model organisms for research, and correcting disease mutations.[1] Early gene editing systems such as Transcription Activator-Like Effector Nucleases (TALEN) and Zinc-Finger Nucleases (ZFN) are effective, but are cumbersome in design and can be expensive to implement.[2] On the other hand, clustered regularly interspaced short palindromic repeats and CRISPR-associated protein 9 (CRISPR/Cas9) is easier to exploit and relatively inexpensive. The CRISPR/Cas9 system utilizes a guide RNA (gRNA) which targets the Cas9 endonuclease to a specific site in the genome which creates a double stranded DNA break (DSB).[3] The cell can repair DSBs through the endogenous DNA repair machinery, non-homologous end joining (NHEJ), or through homology directed repair (HDR) using template DNA in cycling cells.[4]

The application of CRISPR/Cas9 offers enormous possibilities for treating monogenic diseases such as the muscular dystrophies, which are a group of inherited muscle disorders. One of the most devastating lethal muscular dystrophies is Duchenne muscular dystrophy (DMD). DMD is caused by out-of-frame mutations in the DMD gene resulting

M. R. Emami, Dr. A. D. Pyle, Dr. M. J. Spencer
Molecular Biology Institute
University of California, Los Angeles
Los Angeles, CA 90095, USA
E-mail: apyle@mednet.ucla.edu; MSpencer@mednet.ucla.edu
M. R. Emami, Dr. C. S. Young, Dr. E. Mokhonova, Dr. A. D. Pyle,
Dr. M. J. Spencer
Center for Duchenne Muscular Dystrophy
University of California, Los Angeles
Los Angeles, CA 90095, USA

M. R. Emami, Dr. C. S. Young, Dr. A. D. Pyle, Dr. M. J. Spencer
Eli and Edythe Broad Center of Regenerative Medicine and Stem Cell
Research
University of California, Los Angeles
Los Angeles, CA 90095, USA

Dr. C. S. Young, Dr. E. Mokhonova, Dr. M. J. Spencer
Department of Neurology
University of California, Los Angeles
Los Angeles, CA 90095, USA

Dr. Y. Ji, Dr. X. Liu, Dr. H. Meng
Division of Nanomedicine, Department of Medicine
California NanoSystems Institute
University of California, Los Angeles
Los Angeles, CA 90095, USA
E-mail: hmeng@mednet.ucla.edu

Dr. A. D. Pyle
Department of Microbiology, Immunology, and Molecular Genetics
University of California, Los Angeles
Los Angeles, CA 90095, USA

in lack of the dystrophin protein, which leads to progressive muscle wasting and premature death.[5] Thus, a promising therapeutic approach for Duchenne is to restore the reading frame by converting an out-of-frame DMD mutation into an in-frame mutation, mimicking the milder, allelic disease, Becker muscular dystrophy.[6] This approach allows production of an internally deleted but functional dystrophin protein. We have developed a CRISPR/Cas9 platform with the intent to permanently restore the DMD reading frame for mutations within this region.[7] The platform (hereafter referred to as CRISPR DMD$^{\Delta 45\text{-}55}$) encompasses a single pair of gRNAs that flank DMD exons 45–55, generating an in-frame, internally deleted protein after Cas9 cutting and NHEJ. In Becker patients, an exon 45–55 deletion is associated with one of the mildest clinical phenotypes, with some patients still asymptomatic into their 60s.[8] This region also encompasses a hotspot of DMD patient mutations and would be applicable to approximately 50% of the patient population.[8a,8b] Proof-of-principle that CRISPR DMD$^{\Delta 45\text{-}55}$ can restore dystrophin protein was demonstrated in vitro and after local delivery to skeletal muscle in a humanized dystrophic hDMD del45 mdx mouse model in vivo.[7b]

Delivery of CRISPR/Cas9 to muscle has been accomplished in vitro and in vivo via both viral and nonviral strategies. Viral vectors, such as adeno-associated virus (AAV), have been used to deliver CRISPR/Cas9 to various tissues in vivo including muscle.[9] However, since AAV elicits an immune response, it is likely that AAV can only be delivered one time, unless additional procedures are implemented, thus compromising the efficacy of CRISPR-based therapies.[10] Additionally, it has been reported that up to 70% of patients could have pre-existing immunity to AAV, which may limit it's efficacy as a therapy.[11] Moreover, the AAV vector genome has been reported to persist as an episome for years in post-mitotic muscle.[12] This sustained expression of bacterially derived Cas9 has the potential to enhance off-target activity or to prompt an immune response against Cas9 and the muscle.[13] Lastly, because the AAV payload capacity is limited (approximately 4.7kb), it is challenging to fit SpCas9 (approximately 4kb) and gRNAs in the same vector, thus often necessitating a dual vector system, which effectively cuts the maximum dose in half.[14] Nonviral carriers, such as nanoparticles, can overcome the challenges associated with AAV delivery and thus represent a promising alternative for CRISPR delivery.[15] Depending on the type of material used, nanocarriers have the ability to carry different types of cargo and can be chemically modified for colloidal stability, biodegradability, biocompatibility, and tissue specificity. In addition, they are largely non-immunogenic and are suitable for repeat dosing.[16] Nanoparticles composed of lipids, DNA (nanoclews), gold, cationic polymers, and metal-organic frameworks (MOFs) have been used to deliver CRISPR in vitro and in vivo, although reports of nanocarrier mediated delivery of CRISPR to skeletal muscle have been minimal.[17] One study achieved delivery of CRISPR/Cas9 to murine muscle cells in vitro using gold nanoparticles. They also carried out local intramuscular injection in vivo with an efficiency of less than 1%.[17d] However, the translatability of this approach as a DMD therapy is low, as it did not utilize systemic delivery.[17d]

Additional studies have described nano-mediated approaches to deliver other types of cargo to skeletal muscle. Liposomes, polymerosomes, polyethyleneimine (PEI), poly(methyl methacrylate) (PMMA), atelocollagen, perfluorocarbons, and silver nanoparticles have been used to deliver antisense oligonucleotides, rapamycin, siRNA against myostatin, or other genes to muscle.[18] However, these reports have been fairly limited, mainly showing proof-of-concept without much optimization and it is unclear whether the nanoparticles could be modified to carry a large payload, such as CRISPR/Cas9.
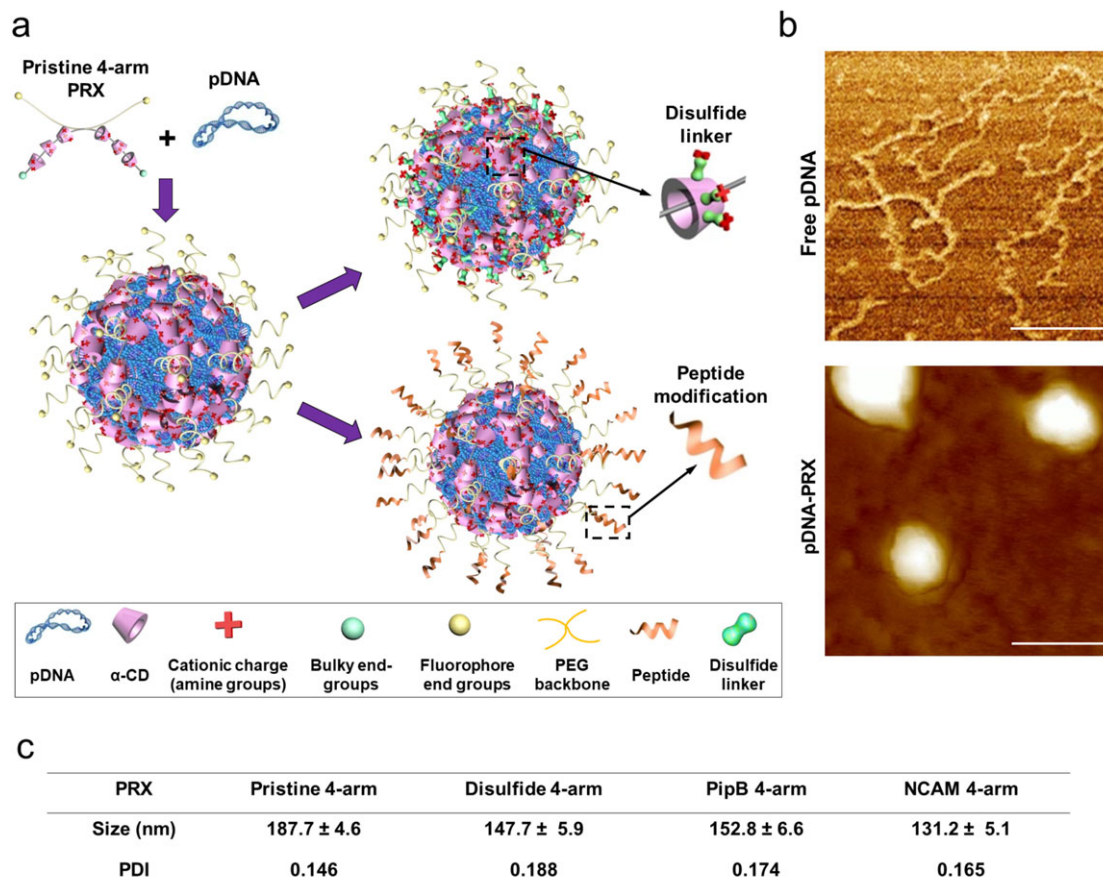
The current work describes the iterative optimization of polyrotaxane (PRX) nanoparticles and demonstrates that PRXs can deliver a large plasmid carrying CRISPR DMD$^{\Delta 45\text{-}55}$ to dystrophic muscle cells in vitro. PRX is characterized as a mechanically interlocked molecule containing a polymer, such as a polyethylene glycol (PEG) backbone, with macrocycles, such as cyclodextrin (CD) rings, threaded onto the polymer and stabilized by bulky end groups.[19] The addition of cationic charge on the macrocycles allows for effective complexation of nucleic acid mediated by electrostatic interactions. We custom-designed a 4-arm PRX nanocarrier that was engineered for improved circulation and pharmacokinetics (PK) following intravenous (IV) injection.[20] This report demonstrates iterative improvements on the 4-arm PRX design to enhance plasmid delivery to primary muscle cells derived from a novel humanized dystrophic mouse model, which contains an out-of-frame human DMD gene.[7b] Engineering the 4-arm PRX with a redox-sensitive disulfide linker improves plasmid release and peptide conjugation enhances the rate and abundance of nanoparticle uptake, which leads to improved gene delivery in vitro. The data also demonstrate proof-of-concept that 4-arm PRX nanoparticles can deliver CRISPR/Cas9 to muscle cells and achieve a CRISPR-mediated deletion of DMD exons 45–55. This highlights the potential of using 4-arm PRXs for a CRISPR-based therapy for DMD.

2. Results and Discussion

2.1. Design and Optimization of 4-Arm PRX Nanoparticles

We have recently demonstrated effective delivery of a plasmid encoding interleukin (IL) in a cancer model using pristine 4-arm PRXs, which had improved gene delivery compared to the classic linear PRX.[20] Enhanced gene delivery of pristine 4-arm PRX was due to the addition of α-cyclodextrin (CD) rings in a spatially and selective fashion onto only two out of the four PEG arms, which increased PEGylation density, thereby enhancing circulation time after IV administration while maintaining encapsulation of nucleic acid mediated by electrostatic interactions (**Figure 1**a). Unlike the pristine 4-arm PRX, the classic linear PRX complexed with nucleic acid results in low PEGylation density, formation of a protein corona, opsonization, and clearance by the reticuloendothelial system (RES).[20]

The pristine 4-arm PRX was synthesized through previously optimized steps, namely 1) bulky end-group protection on 4-arm PEG-tetra-amine, 2) α-CD threading in saturated sugar aqueous solution, 3) use of an amide coupling reaction to introduce Z-L-tyrosine for PRX stabilization, and 4) amine functionalization (Figure S1, Supporting Information).[20] Here, we develop iterations of 4-arm PRXs and optimize delivery of large plasmid cargo to primary dystrophic muscle cells. The first approach was to add a redox-responsive disulfide linker between the cationic amine

**ADVANCED
SCIENCE NEWS**

www.advancedsciencenews.com
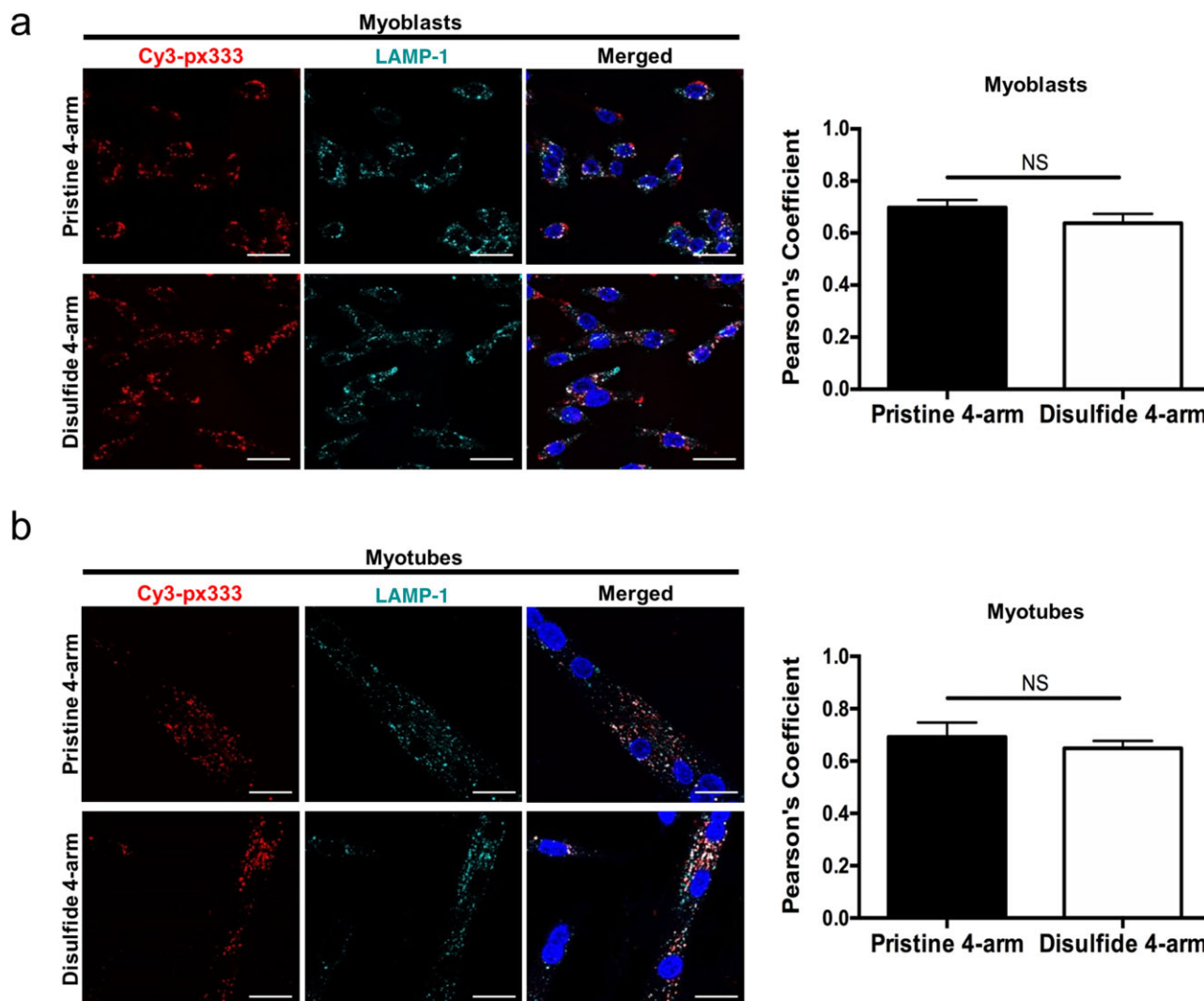
**ADVANCED
THERAPEUTICS**

www.advtherap.com

Figure 1. Design and optimization of the pristine 4-arm PRX nanoparticle. a) Cartoon depicting the 4-arm PRX design containing a 4-arm PEG chain (in yellow) with positively charged α-CD rings (in pink). When plasmid DNA (pDNA) is added (in blue) the positively charged PRX and negatively charged nucleic acids self-assemble. 4-arm PRXs can be modified to include a redox-responsive disulfide linker (in green) or conjugated with peptides (in orange) for cell targeting. b) Atomic force microscopy images of free plasmid encoding CRISPR DMD$^{\Delta 45\text{-}55}$ before (top) and after nanoparticle formation with 4-arm PRX (bottom). Scale bar represented as 200 nm. c) Summary of physiochemical properties, size, and polydispersity (PDI) of all 4-arm PRX formulations.

group and the α-CD ring, whereby cleavage leads to dissociation of the positive charge (Figure 1a, hereafter referred to as disulfide 4-arm PRX). For comparison, pristine linear and disulfide linear PRXs were also made (Figure S2, Supporting Information). In the second approach, two different peptides were conjugated to the nanocarriers to improve targeting and muscle cell uptake (Figure 1a). One is a cell-penetrating peptide (PipB) that has been shown to improve antisense oligonucleotide uptake to muscle.[21] The second involves coupling a synthetic ligand that interacts with neural cell adhesion molecule (NCAM), which is a receptor expressed on muscle cells, including muscle stem cells.[22]

A representative image from atomic force microscopy (AFM) demonstrates self-assembly of a plasmid encoding CRISPR DMD$^{\Delta 45\text{-}55}$ with 4-arm PRX (Figure 1b). All PRX nanocarriers were extensively characterized for size, zeta-potential, number of CD rings, and optimized for plasmid loading (Figures S3 and S4, Supporting Information). The optimal N/P ratio for each formulation was determined from an in vitro reporter assay using a td-Tomato plasmid (Figure S5, Supporting Information). The size and polydispersity index (PDI) of each 4-arm PRX at the optimized N/P ratio are described (Figure 1c).

2.2. Addition of Disulfide-Sensitive Linker in PRX Mediates Plasmid Release in hDMD del45 mdx Murine Muscle Cells

We tested the ability of pristine and disulfide 4-arm PRXs to enter muscle cells and subsequently escape the lysosome. For this analysis, primary murine myoblasts (MB) and myotubes (MT) were obtained from the hDMD del45 mdx mouse.[7b] This model contains a human DMD gene with an exon 45 deletion, which is a region of the gene targeted by CRISPR DMD$^{\Delta 45\text{-}55}$.[7a] Pristine and disulfide 4-arm PRXs exhibited efficient plasmid uptake and were able to escape the lysosome in MB and MT (**Figure 2**). Pearson's correlation coefficient (PCC) of overlap between a lysosomal marker (LAMP-1) and labeled CRISPR/Cas9 plasmid demonstrated a PCC index of less than 0.7 for all PRXs, suggesting an ability to escape the lysosome at 24 h (Figure 2). The pristine linear and disulfide linear PRXs demonstrated similar uptake and lysosomal escape as measured by PCC (Figure S6, Supporting Information). Furthermore, the lack of difference in lysosomal escape between the pristine and disulfide designs was anticipated, as the disulfide linker was designed for a plasmid release mechanism only. Instead, PRXs

**ADVANCED
SCIENCE NEWS**

www.advancedsciencenews.com

**ADVANCED
THERAPEUTICS**

www.advtherap.com

Figure 2. Pristine and disulfide 4-arm PRXs are efficiently taken up and can escape the lysosome in muscle cells in vitro. a,b) Confocal microscopy images of intracellular trafficking of pristine 4-arm and disulfide 4-arm PRX nanoparticles carrying Cy3-labeled CRISPR plasmid (red) and stained with lysosomal marker, LAMP-1 (cyan), and DAPI (blue) in hDMD del45 mdx myoblasts (MB) and myotubes (MT) at 24 h. Scale bar represented as 25 μm. Pearson's correlation coefficient (PCC) quantification between plasmid and LAMP-1 co-localization for pristine 4-arm and disulfide 4-arm PRXs in MB and MT. A lower correlation coefficient demonstrates a dissociation between Cy3 plasmid and LAMP-1 signals. Scale bar represented as 25 μm. Graphs depict average ± standard error of the mean (SEM). NS: not significant.

may be able to escape the lysosomal compartment due to the "proton sponge" effect which has remained a hypothesis and a generally accepted mechanism for cationic polyplexes.[23]

The disulfide-sensitive linker is expected to enhance plasmid release in vitro resulting in a supramolecular dissociation upon exposure to the intracellular reducing environment. The disulfide linker was added to the positively charged α-CD amine groups by thiol-exchange reaction between pyridyldithiol-4-arm polyrotaxane and dimethylamino ethanethiol in aqueous solution (**Figure 3**a and Figure S7, Supporting Information). The addition of the disulfide linker was confirmed using ^{1}H-NMR for the intermediate precursor and final product (Figure S8, Supporting Information). Abiotic assessment of the redox-responsive linker was tested by comparing pristine and disulfide 4-arm PRXs before and after incubation with 5 mM dithiothre-

itol (DTT) for 30 min. We measured a shift in size suggesting dissociation between disulfide 4-arm PRX and plasmid while no change in size was observed for pristine 4-arm PRX (Figure 3b). Furthermore, a gel retardation assay of the disulfide 4-arm PRX incubated with 2.5 mM and 5 mM DTT showed successful plasmid release (Figure S3e, Supporting Information). To validate plasmid release in vitro, co-localization of the plasmid cargo (labeled with Cy3) and PRXs (labeled with FITC) was examined in hDMD del45 murine MB and MT. We observed almost complete co-localization (PCC value of 0.9) between the labeled FITC-pristine 4-arm PRX and Cy3-plasmid cargo in MB and MT 24 h after incubation, which suggests that the nanoparticle did not release the plasmid (Figure 3c,d). As expected, the disulfide 4-arm PRX showed significantly enhanced dissociation in MB and MT 24 h after incubation (PCC value of 0.63). These data suggest that
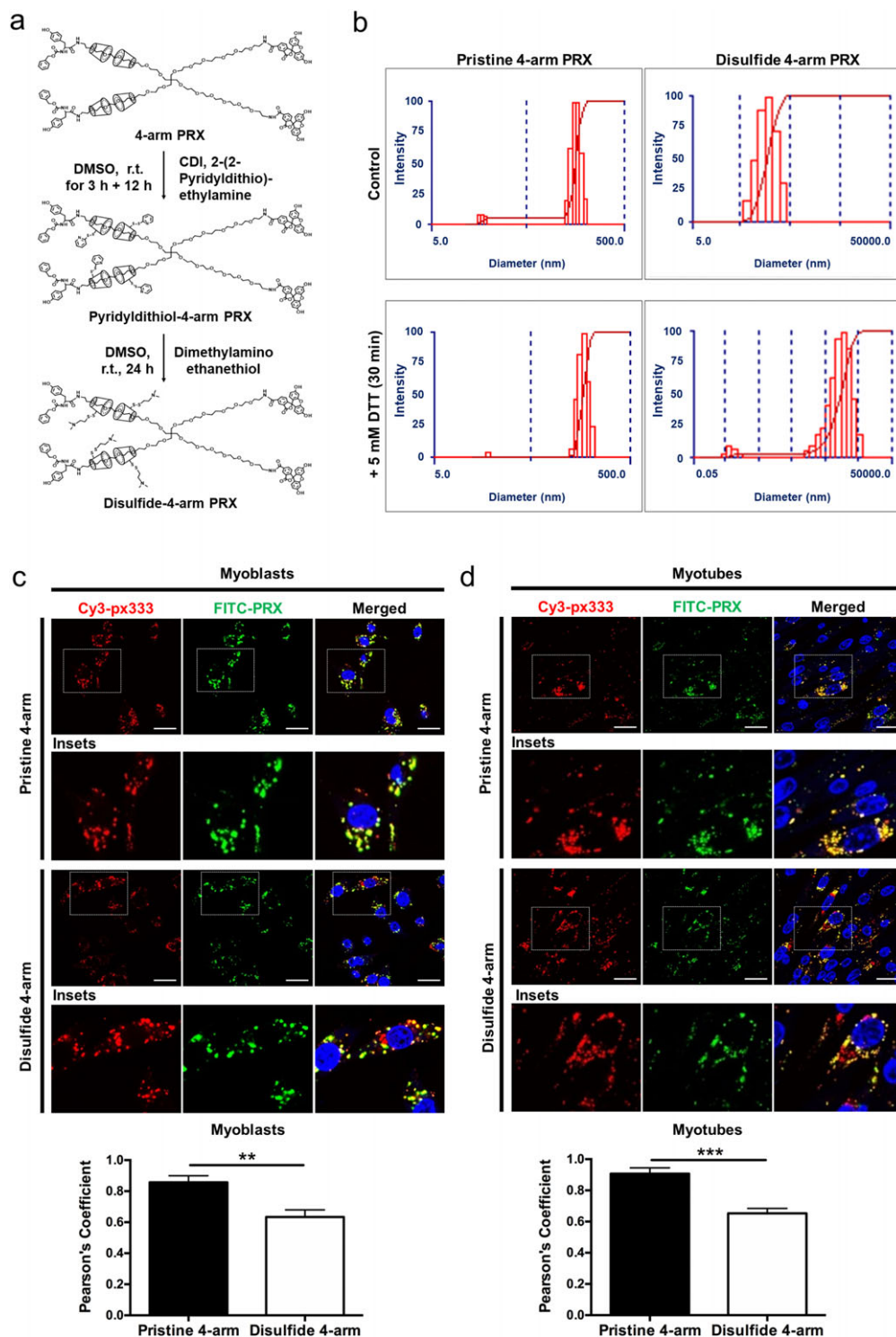
Figure 3. Addition of redox-sensitive disulfide linker mediates plasmid release abiotically and in vitro. a) Synthesis scheme for disulfide 4-arm PRX. Two arms of 4-arm PEG were selectively threaded with α-CD rings and further functionalized with pyridyldithiol groups. Tertiary amines were then conjugated via thiol-exchange chemistry with dimethylamino ethanethiol. The disulfide 4-arm PRX was designed to facilitate intracellular plasmid release in response to a redox signal. b) Size characterization of CRISPR plasmid laden disulfide 4-arm PRX before and after incubation with 5 mM DTT (reducing reagent). The significant change in particle size demonstrated the redox-responsive dissociation of CRISPR plasmid with the disulfide 4-arm PRX. c,d) Confocal microscopy images of pristine 4-arm and disulfide 4-arm PRX nanoparticles labeled with FITC (green) containing Cy3-labeled CRISPR plasmid cargo (red) 24 h after administration in hDMD del45 MB and MT. PCC quantification of PRX and plasmid co-localization with pristine 4-arm and disulfide 4-arm PRX showing reduced co-localization in disulfide 4-arm PRXs demonstrating increased plasmid release (in red). Scale bar represented as 25 µm. Graphs depict average ± standard error of the mean (SEM). NS: not significant; *$p < 0.05$; **$p < 0.01$; ***$p = 0.0001$.
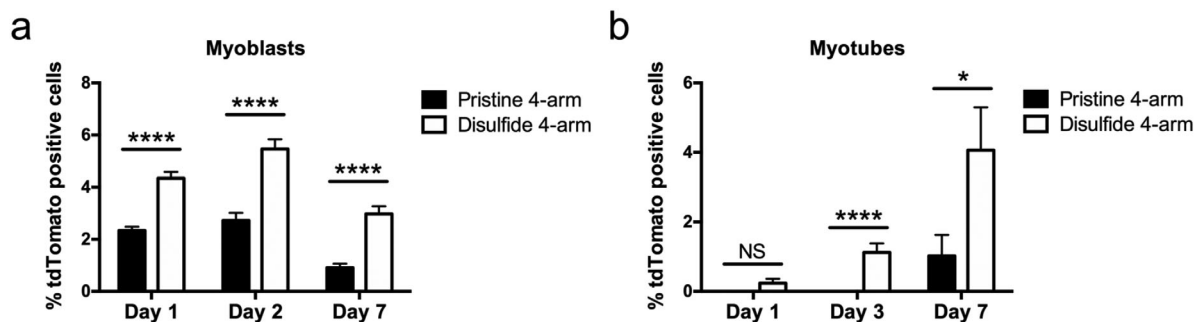
Figure 4. Pristine and disulfide 4-arm PRX nanoparticles successfully deliver tdTomato reporter plasmid to muscle cells in vitro. a,b) Transfection efficiencies of pristine and disulfide 4-arm PRX nanoparticles carrying tdTomato reporter plasmid in hDMD del45 mdx MB measured at days 1, 2, and 7 or in hDMD del45 mdx MT measured at days 1, 3, and 7. Transfection efficiency was assessed in triplicate across two independent experiments. Graphs depict average ± standard error of the mean (SEM). NS: not significant; $*p < 0.05$; $**p < 0.01$; $***p = 0.0001$; $****p < 0.0001$.

addition of a disulfide-linker enhances plasmid release in mammalian cells, which are reported to have pools of reducing agents, such as intracellular glutathione (GSH: approximately 5 mM).[24]

We next assessed whether the released plasmid cargo could traffic to the nucleus by measuring tdTomato reporter protein gene expression in MB and MT (Figure S9, Supporting Information). Pristine and disulfide PRXs were packaged with a tdTomato reporter plasmid and were added to primary MB and MT and the percent of tdTomato positive cells was assessed at time points from 24 h to 7 days. Disulfide linear and disulfide 4-arm PRXs demonstrated significantly greater tdTomato positive MB at days 1, 2, and 7 (**Figure 4**a and Figure S10a, Supporting Information). Likewise, there was a significant increase in tdTomato positive MT with the disulfide 4-arm PRX at days 3 and 7 (Figure 4b). While a slight trend of increased tdTomato was observed in td-Tomato positive MT with the disulfide linear PRX, it was not significantly different (Figure S10b, Supporting Information). This observation suggests the limiting factor of transfection efficiency in MT may not be plasmid release. Instead, the inability of the disulfide linker to significantly increase tdTomato positive MT could be due to a lack of nuclear targeting since myotubes are non-dividing and do not undergo nuclear breakdown.[25]

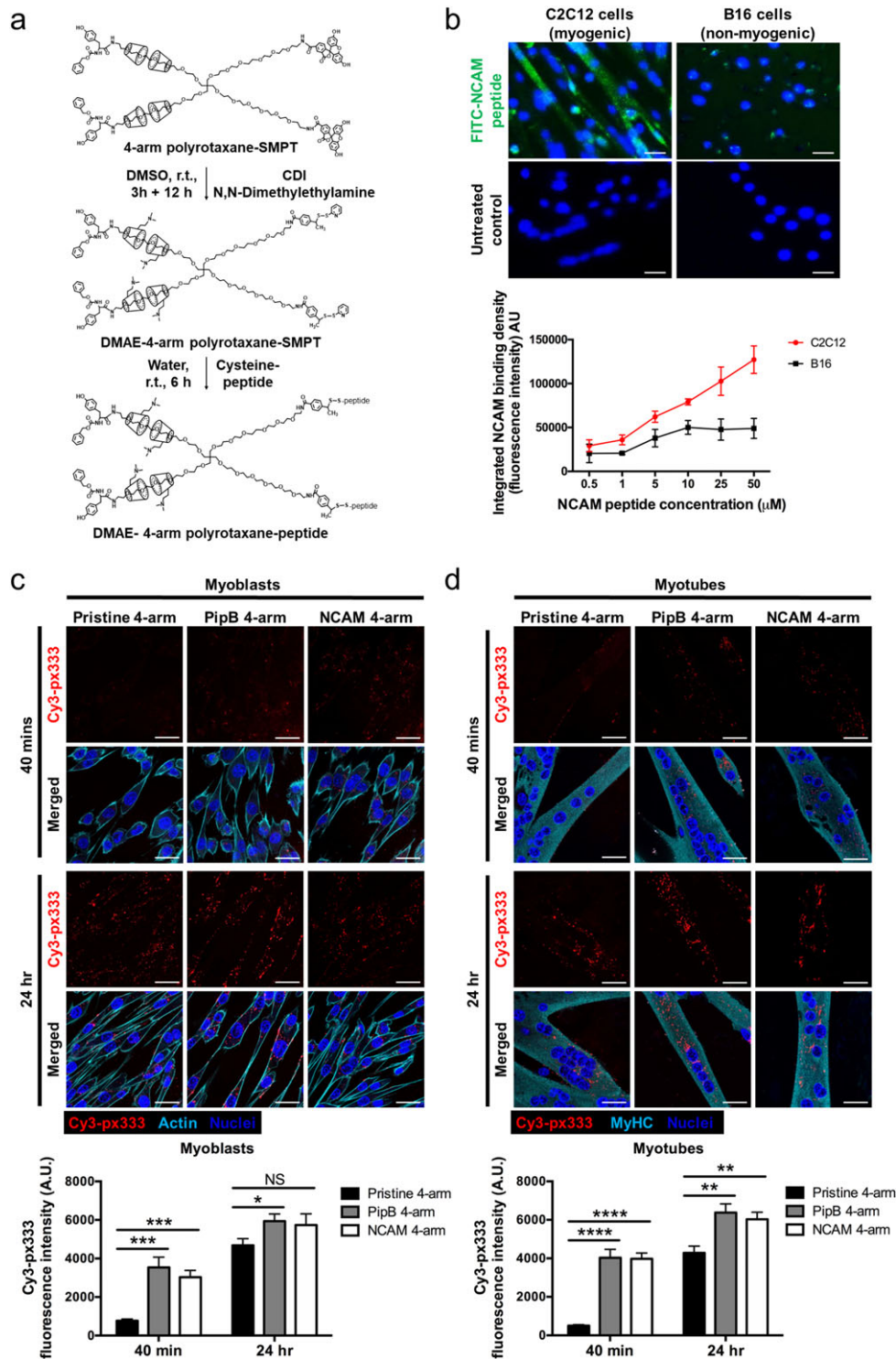### 2.3. Peptide Conjugation to 4-Arm PRXs Enhance Plasmid Delivery to Muscle Cells

In order to improve the specificity and efficacy of PRX delivery to muscle, peptides were conjugated to the nanocarriers. Peptides were modified with cysteine and glycine spacers and were conjugated to the end of free PEG chains in DMAE-4-arm polyrotaxane-SMPT via thiol exchange chemistry on to the pristine 4-arm PRX (**Figure 5**a and Figure S11, Supporting Information). Peptide modifications were confirmed using UV–vis and ^{1}H-NMR (Figure S12, Supporting Information). We were unable to conjugate peptides onto the disulfide 4-arm PRX since disulfide and peptide conjugation utilize the same thiol exchange reaction and thus the chemistry is technically challenging. However, two peptide-modified versions of pristine 4-arm PRX were generated to aid in muscle targeting. Since targeting muscle stem cells is desirable for long term therapeutic efficacy of CRISPR reframing, a ligand for NCAM was conjugated to nanoparticles, since NCAM

is known to be expressed on muscle cells, including both human muscle stem cells and activated mouse muscle stem cells (referred to as NCAM peptide).[26] Another peptide, PipB, was conjugated to nanocarriers since PipB is a cell penetrating peptide shown to increase phosphorodiamidate morpholino oligonucleotide (PMO) uptake in muscle.[21]

NCAM binding to muscle cells was first validated in vitro by incubating a FITC-labeled NCAM peptide with an immortalized mouse muscle cell line, C2C12. C2C12 cells were differentiated to MT, which increase expression of NCAM right after myotube fusion.[22,27] Peptide binding was shown by enhanced FITC signal on C2C12s but not on the negative control cells, NCAM negative, B16 murine cancer cells (Figure 5b).
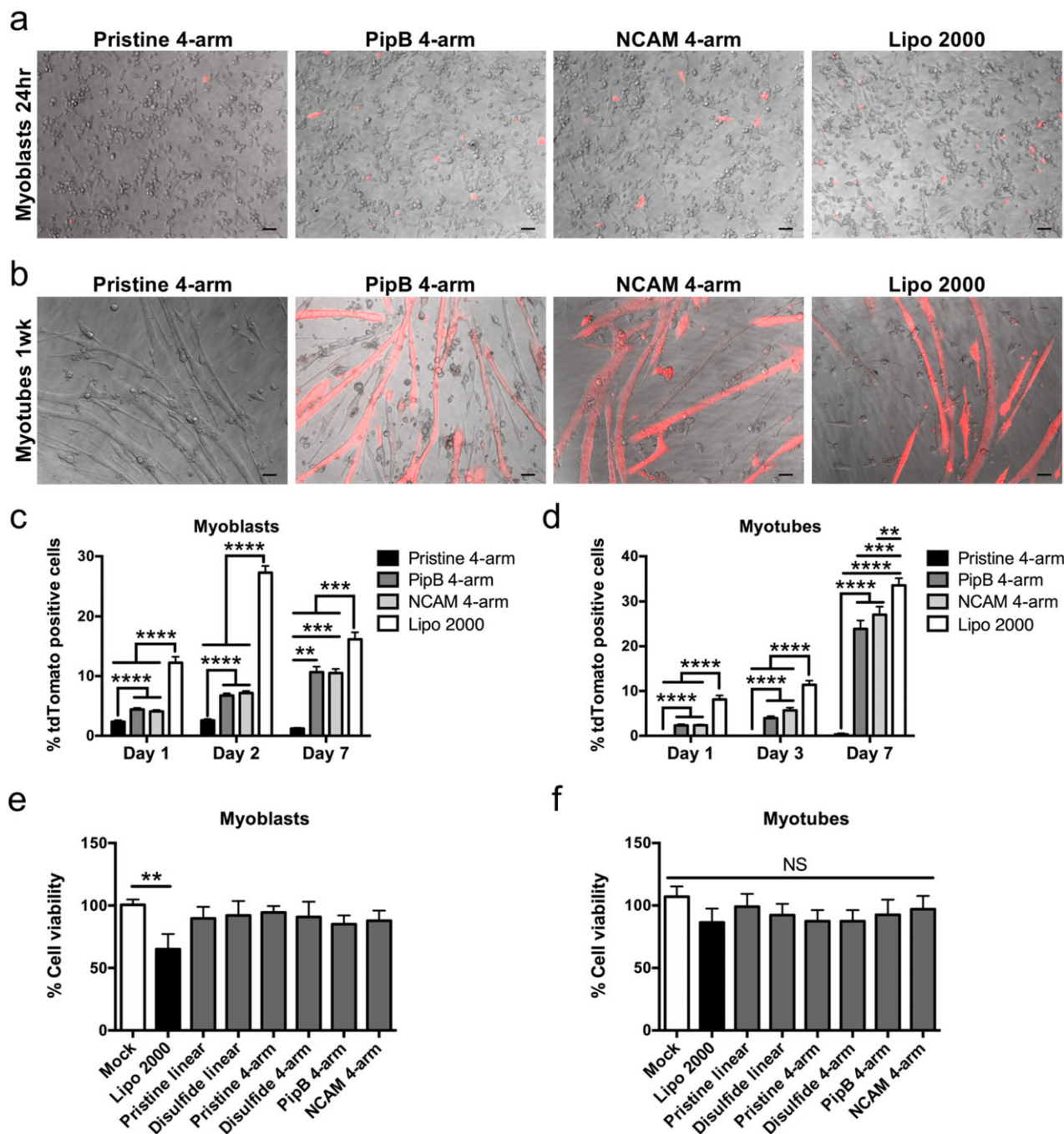
Uptake of the peptide-modified nanocarriers was then tested in primary MB and MT compared to pristine 4-arm PRX. We observed that both peptide conjugated 4-arm PRXs were able to escape the lysosome 24 h post-incubation (Figure S13, Supporting Information). In addition, we observed that PipB 4-arm and NCAM 4-arm PRXs had faster plasmid uptake in vitro than the pristine 4-arm PRX (Figure 5c,d). There was significantly more intracellular labeled plasmid cargo observed 40 min after administration in cells incubated with peptide conjugated versions compared to pristine. By 24 h, this difference was less noticeable, although in MB, PipB 4-arm still had significantly more labeled plasmid cargo and both PipB 4-arm and NCAM 4-arm had more plasmid cargo in MT. Thus, both peptides are able to increase nanoparticle uptake in MB and MT in vitro and both do so to a similar extent.

As a more relevant readout of peptide conjugated 4-arm PRX gene delivery efficiency, we used tdTomato plasmid cargo and examined reporter protein expression in muscle cells 24 h to 7 days post-administration compared to reporter expression after delivery with the lipid-based Lipofectamine 2000 (Lipo 2000) transfection reagent. (**Figure 6**a,b and Figure S14, Supporting Information). Lipo 2000 yielded up to 16% and 33% tdTomato positive MB and MT at 1 week, respectively (Figure 6c,d). Peptide conjugation resulted in a approximately ninefold improvement of reporter expression when compared to the pristine 4-arm PRX, with up to 11% tdTomato positive MB for PipB and NCAM 4-arm PRXs at 1 week (Figure 6c). Furthermore, peptide conjugation resulted in up to 27% and 24% tdTomato positive MT for NCAM and PipB 4-arm PRXs, respectively at 1 week, which

**ADVANCED
SCIENCE NEWS**

www.advancedsciencenews.com

**ADVANCED
THERAPEUTICS**

www.advtherap.com

Figure 5. Peptide conjugated PRXs enhance the rate and abundance of nanoparticle uptake. a) Synthesis scheme for PipB and NCAM peptide conjugation on pristine 4-arm PRX. The cysteine modified peptide (NCAM peptide or PipB peptide) was conjugated through a thiol exchange reaction. b) Imaging of an NCAM peptide labeled with FITC added to C2C12 myotubes or B16 cancer cells (non-muscle cell controls) for 6 h. Quantification of fluorescence intensity of NCAM peptide on C2C12s is compared to B16 controls across various concentrations of peptide. c,d) Confocal microscopy images of intracellular trafficking of pristine 4-arm, PipB 4-arm, and NCAM 4-arm PRX nanoparticles carrying Cy3-labeled plasmid (red) in hDMD del45 mdx MB and MT stained with DAPI (blue) and actin (phalloidin, cyan) or myosin heavy chain (MyHC, cyan), respectively. Imaging is shown at 40 min and 24 h post-administration. Quantification of Cy3 plasmid intensity in MB and MT at 40 min and 24 h post-administration is shown to demonstrate enhanced uptake with peptide conjugation. Scale bar represented as 25 μm. Graphs depict average ± standard error of the mean (SEM). NS: not significant; *$p < 0.05$; **$p < 0.01$; ***$p = 0.0001$; ****$p < 0.0001$.

**ADVANCED
SCIENCE NEWS**

www.advancedsciencenews.com
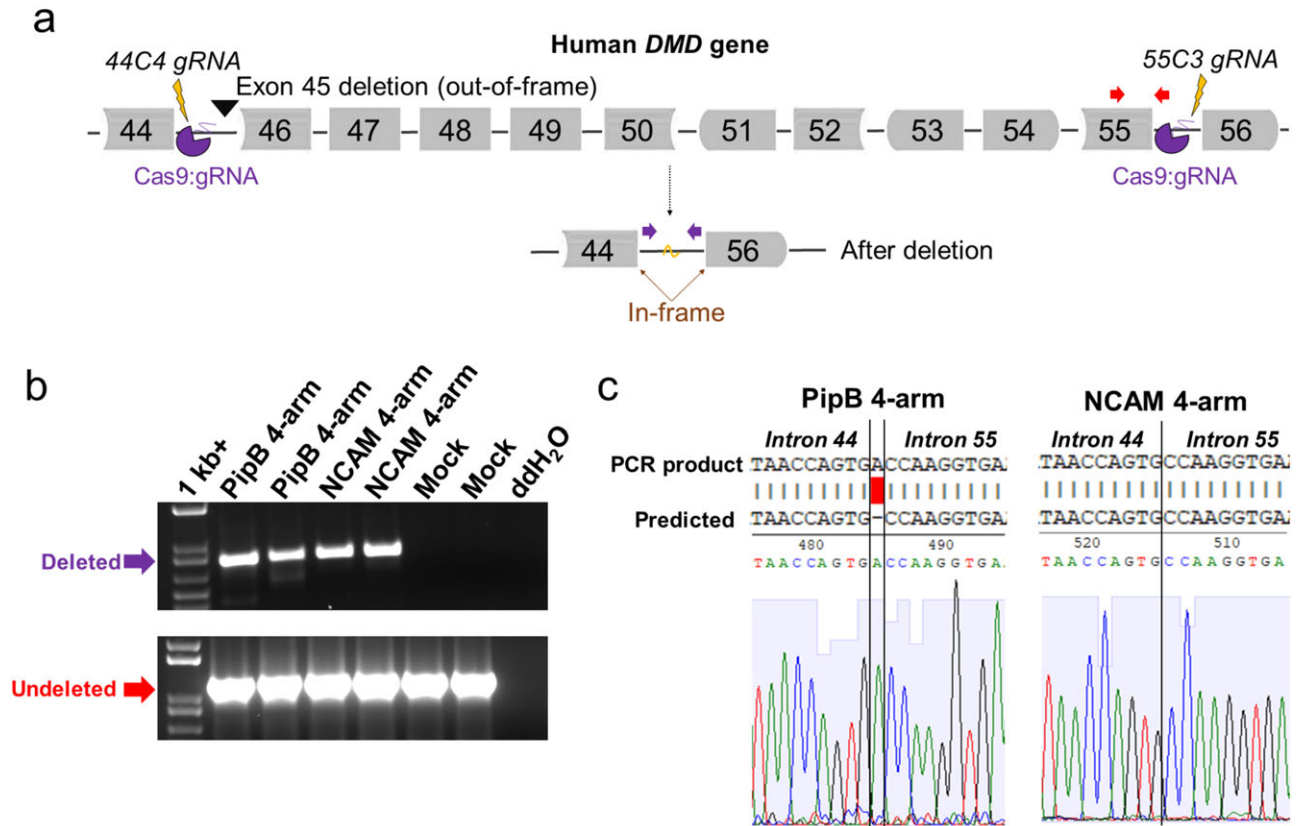
**ADVANCED
THERAPEUTICS**

www.advtherap.com

Figure 6. Peptide conjugated PRXs enhance transfection efficiency in vitro. a,b) Representative images of tdTomato expression (red) merged with brightfield across pristine 4-arm, PipB 4-arm, NCAM 4-arm PRX nanoparticles, and Lipofectamine 2000 carrying tdTomato reporter plasmid in hDMD del45 MB at day 1 and hDMD del45 MT at day 7. Scale bar represented as 50 µm. c,d) Transfection efficiencies of pristine 4-arm, PipB 4-arm, NCAM 4-arm PRXs, and Lipofectamine 2000 measured at days 1, 2, and 7 or days 1, 3, and 7, respectively. Transfection efficiency was assessed in triplicate across two independent experiments. Graphs depict average ± standard error of the mean (SEM). e,f) Cell viability determined by MTS assay of hDMD del45 MB and MT treated with all PRX formulations and Lipofectamine 2000 24 and 72 h post-treatment, respectively. Cell viability was assessed in triplicate. Graphs depict average ± standard deviation (SD). NS: not significant; *$p < 0.05$; **$p < 0.01$; ***$p = 0.0001$; ****$p < 0.0001$.

significantly improved reporter expression by approximately 85-fold compared to the pristine 4-arm PRX (Figure 6d). The enhanced uptake observed with the peptide-modified 4-arm PRXs support the increased tdTomato transfection results.

Next, the cytotoxicity of all PRX formulations and Lipo 2000 was assessed on primary MB and MT by MTS colorimetric assay. The same concentration of PRXs complexed with the CRISPR plasmid was added to primary murine MB and MT in vitro and

**ADVANCED
SCIENCE NEWS**
www.advancedsciencenews.com

**ADVANCED
THERAPEUTICS**
www.advtherap.com

Figure 7. Efficient CRISPR/Cas9 editing of DMD exons 45–55 in primary hDMD del45 mdx muscle cells after PipB 4-arm and NCAM 4-arm PRX delivery. a) Cartoon depicting the region of the human DMD gene (not to scale) in hDMD del45 mdx muscle cells targeted for CRISPR/Cas9 deletion. One gRNA to intron 44 and one to intron 55 target the Cas9 nuclease to generate double stranded breaks and result in removal of exons 45–55. This creates an in-frame deletion that restores the reading frame for the out-of-frame exon 45 deletion (black arrow head). b) PCR on genomic DNA to detect successful deletion of exons 45–55. One primer pair (purple arrows in a) flanks the deletion region in introns 44 and 55 and produces a 788bp band when the deletion has occurred. Another primer pair (red arrows in a) is located internal to the deletion and produces a band of 1,201bp for the undeleted allele as a control. Successful deletion of exons 45–55 was seen in MB after CRISPR delivery by PipB 4-arm and NCAM 4-arm PRXs. Untreated (mock) and water only (ddH$_2$O) are also shown. c) Sequencing of the rejoining site revealed successful deletion and rejoining of introns 44 and 55. Example sequences traces are shown demonstrating a 1bp insertion for MB PipB 4-arm and seamless rejoining for MB NCAM 4-arm. These intronic indels are expected to be inconsequential for dystrophin protein production.

cell viability was measured 24 h and 72 h post-incubation, respectively. There was no observed significant difference in the percent viability for PRX treated MB or MT compared to mock treated control cells (Figure 6e,f). However, there was a significant reduction in cell viability for MB treated with Lipo 2000 (65% cell viability), indicative of cytotoxicity which has previously been reported for Lipofectamine transfections.[28] These results suggest that all PRX formulations are not significantly cytotoxic in vitro.

2.4. PRXs Successfully Deliver CRISPR/Cas9 to Humanized Dystrophic Myoblasts and Myotubes In Vitro

PRX efficacy for delivery of a plasmid encoding CRISPR DMD$^{Δ45-55}$ was tested in primary murine MB and MT. CRISPR DMD$^{Δ45-55}$ consists of two gRNAs, one targeted to intron 44 (44C4) and one to intron 55 (55C3), along with SpCas9, that causes deletion of DMD exons 45–55 by NHEJ and reframing of the gene (**Figure 7**a).[7] Delivery of CRISPR DMD$^{Δ45-55}$ using the disulfide linear PRX demonstrated successful deletion of exons

45–55 as determined by genomic DNA PCR using one primer pair internal to the deletion (undeleted) and one flanking the deletion (deleted allele) after 1 week. However, delivery using the pristine linear PRX did not generate a detectable deletion, even up to 2 weeks after administration (Figure S15a, Supporting Information). CRISPR DMD$^{Δ45-55}$ administration using the disulfide 4-arm PRX led to efficient CRISPR/Cas9-mediated deletion at 1 week compared to the pristine 4-arm PRX (Figure S15b, Supporting Information). The enhanced DNA editing observed with the disulfide modified PRXs is likely due to the improved redox-responsive release mechanism of the CRISPR plasmid.

Since the highest tdTomato transfection efficiency was observed with the peptide conjugated 4-arm PRXs (Figure 6), these formulations were also tested for their ability to deliver CRISPR DMD$^{Δ45-55}$. PipB 4-arm and NCAM 4-arm PRXs carrying CRISPR DMD$^{Δ45-55}$ were added to primary hDMD del45 MB and NCAM 4-arm PRXs to MT. Subsequent assessment of genomic DNA at day 5 demonstrated effective deletion of DMD exons 45–55 as analyzed by PCR (Figure 7b and Figure S15c,d, Supporting Information). Sequencing of the rejoining site in the

**ADVANCED
SCIENCE NEWS**

www.advancedsciencenews.com

**ADVANCED
THERAPEUTICS**

www.advtherap.com

deleted product was performed to demonstrate successful deletion and NHEJ of introns 44 and 55. Representative sequencing traces demonstrate a 1bp insertion or seamless rejoining at the junction site, however since these indels are in the middle of the intron we do not expect them to have any detrimental effects, as demonstrated in our prior study (Figure 7c).[7a] Thus, both the peptide-modified 4-arm and disulfide 4-arm PRXs are effective delivery vehicles of DNA to humanized dystrophic muscle cells, including the large CRISPR/Cas9 plasmid.

3. Conclusion

To summarize, 4-arm PRX nanocarriers have been developed and iteratively optimized for efficient delivery of large plasmid cargo such as CRISPR/Cas9, to primary muscle cells. This study highlights the key advantages of PRXs over other nanomaterials, since they are devoid of cytotoxicity, have a large loading capacity, and are chemically tunable to modify their physiochemical properties to enhance the efficiency of gene delivery. Moreover, we expect PRX nanocarriers could likely be adapted for other nucleic acids such as RNA, which is an approach that offers some advantages for CRISPR delivery compared to DNA, since RNA would not have potential for genomic integration and is short-lived, which could reduce the chance of off-target effects. The innovative aspects of this study include the addition of the disulfide-responsive linker, which enhanced plasmid release following cellular uptake, and conjugation of PipB and NCAM peptides, which augmented gene delivery. Furthermore, this study demonstrated proof-of-concept that 4-arm PRX nanocarriers can deliver a previously validated CRISPR/Cas9 gene editing platform to humanized dystrophic muscle cells and achieve deletion of DMD exons 45–55. This work lays a foundation for use of the 4-arm PRX as an efficacious in vitro transfection reagent for muscle cells and sets a path for future in vivo studies.

4. Experimental Section

Cell Culture: Primary hDMD del45 mdx myoblasts were obtained from 11–13 day old pups by dissociation of muscle tissue using a 1:1 mixture of 1.5 mg mL^{-1} dispase (neutral protease, Worthington) and 1600 U mL^{-1} collagenase II (Worthington) in PBS at 200 µL per 100 mg tissue. Muscles were minced, then incubated at 37 °C with slow agitation for 30 min. Fibroblasts were removed by repeatedly pre-plating. Myoblasts were cultured on entactin-collagenIV-laminin cell attachment matrix (ECL, EMD Millipore) and maintained in F-10 HAM (Sigma) with 20% fetal bovine serum (FBS, Thermo Fisher), 5 ng mL^{-1} basic fibroblast growth factor (bFGF, Promega), and 1% penicillin/streptomycin (P/S, Thermo Fisher). Myoblasts were differentiated to form myotubes (at >80% confluence) in DMEM (Thermo Fisher) supplemented with 2% horse serum (Thermo Fisher), 1% insulin-transferrin, selenium (ITS, Thermo Fisher), and 1% P/S on Matrigel basement membrane matrix (Corning). C2C12 murine myoblasts were maintained in DMEM supplemented with 20% FBS and 1% P/S. C2C12 myoblasts were differentiated to form myotubes (at >80% confluence) in DMEM supplemented with 5% horse serum and 1% P/S. B16 murine melanoma cells were maintained in DMEM supplemented with 10% FBS and 1% P/S.

CRISPR Plasmid: gRNAs for the exon 45–55 deletion (44C4, 55C3) from[7a] were cloned into px333 (Addgene 64073, Andrea Ventura[29]) in tandem using BbsI (New England BioLabs) and BsaI (New England BioLabs). Hereafter, px333 44C4+55C3 refers to the CRISPR plasmid encoding SpCas9 and the two gRNAs.

Chemicals: α-Cyclodextrin (α-CD), triethylamine (TEA), Benzyloxycarbonyl-L-tyrosine (Z-L-Tyr), Benzotriazol-1-yl-oxy-tris(dimethylamino) phosphonium hexafluorophosphate (BOP), 1-hydroxybenzotriazole (HOBt,) N,N-diisopropylethylamine (DIEA), 1,1′-carbonyldiimidazole (CDI), N,N-dimethylethylenediamine (DMAE), 2-aminoethanethiol, 1,4-dithiothreitol (DTT) dimethylformamide (DMF), dimethyl sulfoxide (DMSO) were purchased from Sigma-Aldrich. Four-arm PEG tetra-amine hydrochloride salt (10 kDa) and linear PEG-diamine hydrochloride salt (3.5 kDa) were purchased from Jen Kem Technology. Di-orthopyridyl disulfide PEG (PEG-diOPSS) (3.5 kDa) was purchased from Creative PEGworks. NHS-fluorescein and 4-succinimidyloxycaronyl-alpha-methyl-α(2-pyridyldithio)toluene (SMPT) were purchased from Thermo Fisher. 2-(Dimethlamino ethanethiol) hydrochloride was purchased from Santa Cruz Biotechnology. Pyridyldithiol-cysteamine was synthesized as previously described.[30] Amicon Ultra-4 Centrifugal Filter Units (MWCO = 10 kDa) were purchased from Millipore.

PRX Synthesis: For the pristine linear PRX the following steps were completed as previously reported.[31] i) Linear PEG-diamine was added to aqueous saturated solution of α-CDs to form a polypseudorotaxane inclusion complex. ii) The polypseudorotaxane ends were blocked with a large blocking group, Z-L-Tyr, by mixing the inclusion complex with Z-L-Tyr, BOP reagent, HOBt, and DIEA in DMF. iii) The α-CDs in the polyrotaxane were modified with positively charged amine groups by reaction with DMAE and CDI in DMSO.

For the disulfide linear PRX the following steps were completed as previously reported.[32] i) Linear PEG di(OPSS) was mixed with 2-aminoethanethiol to generate a diamino-PEG with disulfide linkages at both ends (SS-PEG-diamine). ii) The SS-PEG-diamine was added to aqueous saturated solution of α-CDs to form an SS-polypseudorotaxane inclusion complex. iii) The polypseudorotaxane ends were blocked with Z-L-Tyr, as done for the pristine linear PRX. iv) The α-CDs in the SS-polyrotaxane were modified with positively charged amine groups by reaction with DMAE and CDI in DMSO.

For the pristine 4-arm PRX the steps were performed as we described previously.[20] i) Two arms of a 4-arm PEG tetra-amine were selectively blocked by NHS-Fluorescein. ii) The 4-arm PEG diamine was then added to aqueous saturated solution of α-CDs to form a 2/4-arm polypypseudorotaxane inclusion complex. iii) The amino ends of 2/4-arm polypseudorotaxane were blocked with Z-L-Tyr as described above. iv) The α-CDs in the 2/4-arm polyrotaxane were modified with positively charged amine groups by reaction with DMAE and CDI in DMSO.

For the disulfide 4-arm PRX the following steps were carried out. i) Two arms of a 4-arm PEG tetra-amine polymer were selectively blocked with NHS-Fluorescein as mentioned above. ii) The 4-arm PEG diamine was added to aqueous saturated solution of α-CDs to form a 2/4-arm polypseudorotaxane inclusion complex. iii) The amino ends of 2/4-arm polypseudorotaxane were blocked with Z-L-Tyr as described above. iv) The α-CDs in the 2/4-arm polyrotaxane were further functionalized with pyriyldithiol groups by reacting with pyridyldithiol-cysteamine and CDI in DMSO, followed by precipitation in diethyl ether, and washed sequentially in excessive acetone and methanol. v) The α-CDs with cleavable positively charged amine groups were generated by thiol-exchange reaction between pyridyldithiol-4-arm polyrotaxane and dimethlamino ethanethiol in aqueous solution. The resulting disulfide 4-arm PRX was concentrated with DI water in Amicon centrifugal filter to remove excessive pyridyldithiol-cysteamine.

For peptide conjugation to 4-arm PRX the following steps were carried out. i) Two arms of a 4-arm PEG tetra-amine polymer were selectively blocked after a reaction with SMPT in DMF at a fixed feed ratio (4-arm PEG:SMPT = 1:2, molar ratio). ii) The 4-arm PEG diamine-SMPT was added to aqueous saturated solution of α-CDs to form a 2/4-arm polypseudorotaxane-SMPT inclusion complex. iii) The amino ends of 2/4–arm polypseudorotaxane-SMPT were blocked with Z-L-Tyr as mentioned above. iv) The α-CDs in the 2/4-arm polyrotaxane were modified with positively charged amine groups by reaction with DMAE and CDI in DMSO as done for pristine 4-arm PRX. v) Peptides modified with cysteine and glycine spacers were conjugated to the ends of free PEG chains in DMAE-4-arm polyrotaxane-SMPT via thiol exchange chemistry.

**ADVANCED
SCIENCE NEWS**

www.advancedsciencenews.com

**ADVANCED
THERAPEUTICS**

www.advtherap.com

The peptide sequences are as follows: NCAM ASKKPKRNIKAGGC, PipB RXRRBRRXRRBRXBGGC.[21,22] Thiol groups from cysteine were introduced on the C-terminus of the peptides to facilitate conjugation. An oligo glycine spacer was included at both ends of the functional sequence so that conjugation would not interfere with the binding efficiency. The modified peptides were mixed with DMAE-4-arm polyrotaxane-SMPT at a molar ratio of 5:1 in aqueous solution and reacted for 2 h at room temperature. The excessive peptide and pyridine-2-thione was removed via repeated concentration with DI water in Amicon centrifugal filter. The pyridine-2-thione was collected and quantified by UV–vis spectroscopy to determine the successful peptide conjugation.

The synthesis schemes for PRX formulations can be found in Figures S1, S7, and S11, Supporting Information.[31,32] For the list of average CD numbers per polymer and cationic charge density (Figure S4, Supporting Information), PRX samples were dissolved in d_6-DMSO or deuterated water and examined on an AV400 spectrometer (Bruker). The integration of C1(H) peak (δa) from α-CD and -CH_2CH_2O- peak (δf) from PEG were used to calculate the total number of α-CD per PRX polymer. The cationic charge density was determined via the integration of -$N(CH_3)_2$ peak (δg) from DMAE and C1(H) peak (δa) from α-CD in ^{1}H-NMR spectra as we reported previously.[20] For peptide conjugated 4-arm PRX, UV–vis spectroscopy was used to confirm peptide conjugation by the production of pyridine-2-thione (Figure S12, Supporting Information). The enhanced absorbance at 340–380 nm demonstrated successful peptide conjugation.

Physiochemical Characterization and Plasmid Loading of PRX Formulations: CRISPR plasmid was complexed with different PRXs at various N/P ratios in aqueous solution with an equivalent plasmid concentration of 1 µg mL^{-1}. The size and ζ-potential of plasmid complexed with different PRXs were measured by ZETAPALS (Brookhaven Instruments Corporation). DNA gel retardation assay was performed with precast agarose gel (Sigma-Aldrich). Samples (equivalent to 100 ng plasmid) were loaded in gel loading buffer (Sigma-Aldrich), ran in TBE buffer at 150 V for 30 min, followed by visualization on gel imager (MultiImage II AlphaImager HP, Alpha Innotech). To demonstrate the reduction-responsive dissociation of plasmid, CRISPR plasmid laden disulfide 4-arm PRXs were incubated with 5 mM DTT solution for 30 min, before assessing size or DNA gel electrophoresis. The morphology of plasmid laden PRX was visualized by atomic force microscopy (AFM). Plasmid laden PRX was directly added to mica substrate (1 cm × 1 cm), and free plasmid was premixed with 5 mM MgCl$_2$-HEPES buffer before addition to mica substrate. The equivalent concentration of plasmid was 0.2 µg mL^{-1}. The samples were dried with nitrogen gas and imaged on Bruker Dimension FastScan AFM.

PRX Delivery In Vitro: Myoblasts were seeded at 1.2×10^5 cells cm^{-2} for growth conditions or 1.7×10^5 cells cm^{-2} for differentiation where the media was changed to differentiation media the following day. PRX complexed with a pCSCMV:tdTomato reporter plasmid (Addgene 30530, Gerhart Ryffel[33]), or px333 44C4+55C3 CRISPR plasmid (see above) was added to the cells at various PRX to plasmid (N/P) ratios determined empirically and as follows: pristine linear PRX to plasmid: 10:1, disulfide linear PRX to plasmid: 5:1, pristine 4-arm, and disulfide 4-arm PRX to plasmid: 3:1, peptide conjugated 4-arm PRX to plasmid: 5:1. For uptake and plasmid dissociation studies, PRXs were conjugated with FITC and plasmid labeled with Cy3 using LabelIT Tracker kit (Mirus Bio). Imaging for uptake and lysosomal studies was done at time points between 40 min and 24 h using a confocal microscope (SP8-SMD, Leica). Imaging for reporter expression was done at time points between 1 day and 7 days using an Axio Observer Z1 microscope (Zeiss) and five random images per well were taken for quantification in ImageJ software (NIH). For CRISPR delivery, cells were harvested at days 5, 7, or 14 and pelleted for genomic DNA extraction using the Quick gDNA mini prep kit (Zymo Research) and analyzed with the deletion PCR described below.

Lipofectamine 2000 Transfection: Lipofectamine 2000 (Invitrogen) transfections were carried out in a 96-well plate according to the manufacturer's instructions. In brief, complexes were prepared by mixing 0.2 µg tdTomato plasmid DNA with 0.5 µL Lipofectamine 2000 (2:5, w/v) per well for myoblasts and myotubes.

CRISPR Exon 45–55 Deletion PCR: To assay for the exon 45–55 deletion, individual PCR reactions containing primers flanking the deletion

(purple arrows in Figure 7a) or internal to the deletion (red arrows in Figure 7a) were performed on genomic DNA using AccuPrime Taq High Fidelity (Thermo Fisher) or Herculase II Fusion Polymerase (Agilent Genomics) as described.[7a] PCR products were blunt cloned with Zero Blunt TOPO according to the manufacturer's instructions and sequenced by Laragen Inc.

NCAM Peptide Administration In Vitro: A green fluorophore (5-FAM on N-terminus) labeled NCAM peptide (sequence ASKKPKRNIKAGGC[22]) was synthesized by Biomatik. 0.5, 1, 5, 10, 25, and 50 µM NCAM peptide was incubated for 6 h on C2C12 and B16 cells before imaging.

Intracellular Uptake Study of Cy-3 Labeled CRISPR Plasmid: The following working antibody concentrations were used: anti-LAMP-1 antibody (Abcam, ab25245) at 1 µg mL^{-1}, anti-myosin 4 antibody MF20 at 2 µg mL^{-1}. Goat anti-rat IgG (H+L) Alexafluor 647 (Thermo Fisher, A21247), and goat anti-mouse IgG (H+L) Alexafluor 647 (Thermo Fisher, A21235) were used as secondary antibodies, respectively. F-actin was stained with Phalloidin-iFluor 647 Reagent (Abcam, ab176759). The nuclei were counterstained with DAPI. The intracellular distribution of Cy3-labeled plasmid was visualized by confocal microscopy (SP8-SMD, Leica). For the image analysis, Pearson's correlation coefficient was used to determine the level of co-localization between LAMP-1/Cy3-plamid or PRX/Cy3-plasmid.[34] Image Pro Plus (Media Cybernetics) software was used to determine Pearson's correlation coefficient ($n = 5$). To evaluate the intracellular level of Cy3-plasmid, the intracellular fluorescence intensity was analyzed by ImageJ software (NIH) ($n = 5$). The fluorescence intensity per image was normalized to cell number in the case of myoblasts or cell spread area in the case of myotubes for comparison.

MTS Colorimetric Assay: Cell viability was measured using the CellTiter 96 Aqueous One Solution MTS assay (Promega) according to the manufacturer's instructions. Measurements were taken 24 h post-administration for myoblasts and 72 h post-administration for myotubes. In brief, cells were treated with 20 uL per well assay reagent and incubated for 2 h at 37 °C. Absorbance (OD = 490 nm) was measured using a microplate reader (M5e, Molecular Device), and normalized to untreated control cells to determine percentage of cell viability ($n = 6$).

Statistical Analysis: Results presented in Figures 2–6 and S6, S10, and S13, Supporting Information, are shown as mean ± standard error of the mean (SEM) and comparison between two conditions was evaluated by the unpaired t-test (two-tailed). Results in Figure 6e and f are presented as mean ± standard deviation (SD) and comparison between groups was evaluated using one-way analysis of variance (ANOVA) followed by Tukey's post-hoc test. $p < 0.05$ (*), $p < 0.01$ (**), $p = 0.0001$ (***), $p < 0.0001$ (****) were considered significant. Statistical analysis and graphs were generated using GraphPad Prism 6 software.

Supporting Information

Supporting Information is available from the Wiley Online Library or from the author.

Acknowledgements

Conflict of Interest

H.M. is a co-founder and equity holder of the Westwood Bioscience Inc. and Nammi Therapeutics Inc. The remaining authors declare no conflict of interest.

Keywords

CRISPR/Cas9, Duchenne muscular dystrophy, muscle, nanoparticle, polyrotaxanes

[1] R. Barrangou, J. A. Doudna, *Nat. Biotechnol.* **2016**, *34*, 933.

[2] J. A. Doudna, E. Charpentier, *Science* **2014**, *346*, 1258096.

[3] a) L. Cong, F. A. Ran, D. Cox, S. Lin, R. Barretto, N. Habib, P. D. Hsu, X. Wu, W. Jiang, L. A. Marraffini, F. Zhang, *Science* **2013**, *339*, 819; b) M. Jinek, K. Chylinski, I. Fonfara, M. Hauer, J. A. Doudna, E. Charpentier, *Science* **2012**, *337*, 816; c) P. Mali, L. Yang, K. M. Esvelt, J. Aach, M. Guell, J. E. DiCarlo, J. E. Norville, G. M. Church, *Science* **2013**, *339*, 823.

[4] M. R. Lieber, *Annu. Rev. Biochem.* **2010**, *79*, 181.

[5] H. Moser, *Hum. Genet.* **1984**, *66*, 17.

[6] A. P. Monaco, C. J. Bertelson, S. Liechti-Gallati, H. Moser, L. M. Kunkel, *Genomics* **1988**, *2*, 90.

[7] a) C. S. Young, M. R. Hicks, N. V. Ermolova, H. Nakano, M. Jan, S. Younesi, S. Karumbayaram, C. Kumagai-Cresse, D. Wang, J. A. Zack, D. B. Kohn, A. Nakano, S. F. Nelson, M. C. Miceli, M. J. Spencer, A. D. Pyle, *Cell Stem Cell* **2016**, *18*, 533; b) C. S. Young, E. Mokhonova, M. Quinonez, A. D. Pyle, M. J. Spencer, *J. Neuromuscul. Dis.* **2017**, *4*, 139.

[8] a) C. Beroud, S. Tuffery-Giraud, M. Matsuo, D. Hamroun, V. Humbertclaude, N. Monnier, M. P. Moizard, M. A. Voelckel, L. M. Calemard, P. Boisseau, M. Blayau, C. Philippe, M. Cossee, M. Pages, F. Rivier, O. Danos, L. Garcia, M. Claustres, *Hum. Mutat.* **2007**, *28*, 196; b) A. Nakamura, N. Shiba, D. Miyazaki, H. Nishizawa, Y. Inaba, N. Fueki, R. Maruyama, Y. Echigoya, T. Yokota, *J. Hum. Genet.* **2017**, *62*, 459; c) A. Nakamura, K. Yoshida, K. Fukushima, H. Ueda, N. Urasawa, J. Koyama, Y. Yazaki, M. Yazaki, T. Sakai, S. Haruta, S. Takeda, S. Ikeda, *J. Clin. Neurosci.* **2008**, *15*, 757; d) A. Taglia, R. Petillo, P. D'Ambrosio, E. Picillo, A. Torella, C. Orsini, M. Ergoli, M. Scutifero, L. Passamano, A. Palladino, G. Nigro, L. Politano, *Acta Myol.* **2015**, *34*, 9. e) M. Yazaki, K. Yoshida, A. Nakamura, J. Koyama, T. Nanba, N. Ohori, S. Ikeda, *Eur. Neurol.* **1999**, *42*, 145.

[9] C. H. Lau, Y. Suh, *F1000Research* **2017**, *6*, 2153.

[10] S. Boutin, V. Monteilhet, P. Veron, C. Leborgne, O. Benveniste, M. F. Montus, C. Masurier, *Hum. Gene Ther.* **2010**, *21*, 704.

[11] V. Louis Jeune, J. A. Joergensen, R. J. Hajjar, T. Weber, *Hum. Gene Ther: Methods* **2013**, *24*, 59.

[12] a) G. Buchlis, G. M. Podsakoff, A. Radu, S. M. Hawk, A. W. Flake, F. Mingozzi, K. A. High, *Blood* **2012**, *119*, 3038; b) C. Le Guiner, L. Servais, M. Montus, T. Larcher, B. Fraysse, S. Moullec, M. Allais, V. Francois, M. Dutilleul, A. Malerba, T. Koo, J. L. Thibaut, B. Matot, M.

Devaux, J. Le Duff, J. Y. Deschamps, I. Barthelemy, S. Blot, I. Testault, K. Wahbi, S. Ederhy, S. Martin, P. Veron, C. Georger, T. Athanasopoulos, C. Masurier, F. Mingozzi, P. Carlier, B. Gjata, J. Y. Hogrel, et al., *Nat. Commun.* **2017**, *8*, 16105.

[13] a) C. T. Charlesworth, P. S. Deshpande, D. P. Dever, J. Camarena, V. T. Lemgart, M. K. Cromer, C. A. Vakulskas, M. A. Collingwood, L. Zhang, N. M. Bode, M. A. Behlke, B. Dejene, B. Cieniewicz, R. Romano, B. J. Lesch, N. Gomez-Ospina, S. Mantri, M. Pavel-Dinu, K. I. Weinberg, M. H. Porteus, *Nat. Med.* **2019**, *25*, 249; b) M. Penaud-Budloo, C. Le Guiner, A. Nowrouzi, A. Toromanoff, Y. Chérel, P. Chenuaud, M. Schmidt, C. von Kalle, F. Rolling, P. Moullier, R. O. Snyder, *J. Virol.* **2008**, *82*, 7875.

[14] J. C. Grieger, R. J. Samulski, *J. Virol.* **2005**, *79*, 9933.

[15] B. E. Givens, Y. W. Naguib, S. M. Geary, E. J. Devor, A. K. Salem, *AAPS J.* **2018**, *20*, 108.

[16] H. Meng, W. Leong, K. W. Leong, C. Chen, Y. Zhao, *Biomaterials* **2018**, *174*, 41.

[17] a) J. D. Finn, A. R. Smith, M. C. Patel, L. Shaw, M. R. Youniss, J. van Heteren, T. Dirstine, C. Ciullo, R. Lescarbeau, J. Seitzer, R. R. Shah, A. Shah, D. Ling, J. Growe, M. Pink, E. Rohde, K. M. Wood, W. E. Salomon, W. F. Harrington, C. Dombrowski, W. R. Strapps, Y. Chang, D. V. Morrissey, *Cell Rep.* **2018**, *22*, 2227; b) J. S. Ha, J. S. Lee, J. Jeong, H. Kim, J. Byun, S. A. Kim, H. J. Lee, H. S. Chung, J. B. Lee, D. R. Ahn, *J. Controlled Release* **2017**, *250*, 27; c) C. Jiang, M. Mei, B. Li, X. Zhu, W. Zu, Y. Tian, Q. Wang, Y. Guo, Y. Dong, X. Tan, *Cell Res.* **2017**, *27*, 440; d) K. Lee, M. Conboy, H. M. Park, F. Jiang, H. J. Kim, M. A. Dewitt, V. A. Mackley, K. Chang, A. Rao, C. Skinner, T. Shobha, M. Mehdipour, H. Liu, W. C. Huang, F. Lan, N. L. Bray, S. Li, J. E. Corn, K. Kataoka, J. A. Doudna, I. Conboy, N. Murthy, *Nat. Biomed. Eng.* **2017**, *1*, 889; e) K. Lee, V. A. Mackley, A. Rao, A. T. Chong, M. A. Dewitt, J. E. Corn, N. Murthy, *eLife* **2017**, *6*, e25312; f) J. B. Miller, S. Zhang, P. Kos, H. Xiong, K. Zhou, S. S. Perelman, H. Zhu, D. J. Siegwart, *Angew. Chem., Int. Ed.* **2017**, *56*, 1059; g) R. Mout, M. Ray, G. Yesilbag Tonga, Y. W. Lee, T. Tay, K. Sasaki, V. M. Rotello, *ACS Nano* **2017**, *11*, 2452; h) W. Sun, W. Ji, J. M. Hall, Q. Hu, C. Wang, C. L. Beisel, Z. Gu, *Angew. Chem., Int. Ed.* **2015**, *54*, 12029; i) A. S. Timin, A. R. Muslimov, K. V. Lepik, O. S. Epifanovskaya, A. I. Shakirova, U. Mock, K. Riecken, M. V. Okilova, V. S. Sergeev, B. V. Afanasyev, B. Fehse, G. B. Sukhorukov, *Nanomedicine* **2018**, *14*, 97; j) M. Wang, J. A. Zuris, F. Meng, H. Rees, S. Sun, P. Deng, Y. Han, X. Gao, D. Pouli, Q. Wu, I. Georgakoudi, D. R. Liu, Q. Xu, *Proc. Natl. Acad. Sci. U. S. A.* **2016**, *113*, 2868; k) H. Yin, C. Q. Song, J. R. Dorkin, L. J. Zhu, Y. Li, Q. Wu, A. Park, J. Yang, S. Suresh, A. Bizhanova, A. Gupta, M. F. Bolukbasi, S. Walsh, R. L. Bogorad, G. Gao, Z. Weng, Y. Dong, V. Koteliansky, S. A. Wolfe, R. Langer, W. Xue, D. G. Anderson, *Nat. Biotechnol.* **2016**, *34*, 328; l) H. Yin, C. Q. Song, S. Suresh, Q. Wu, S. Walsh, L. H. Rhym, E. Mintzer, M. F. Bolukbasi, L. J. Zhu, K. Kauffman, H. Mou, A. Oberholzer, J. Ding, S. Y. Kwan, R. L. Bogorad, T. Zatsepin, V. Koteliansky, S. A. Wolfe, W. Xue, R. Langer, D. G. Anderson, *Nat. Biotechnol.* **2017**, *35*, 1179; m) J. A. Zuris, D. B. Thompson, Y. Shu, J. P. Guilinger, J. L. Bessen, J. H. Hu, M. L. Maeder, J. K. Joung, Z. Y. Chen, D. R. Liu, *Nat. Biotechnol.* **2015**, *33*, 73; n) Z. Chen, F. Liu, Y. Chen, J. Liu, X. Wang, A. T. Chen, G. Deng, H. Zhang, J. Liu, Z. Hong, J. Zhou, *Adv. Funct. Mater.* **2017**, *27*, 1703036; o) S. K. Alsaiari, S. Patil, M. Alyami, K. O. Alamoudi, F. A. Aleisa, J. S. Merzaban, M. Li, N. M. Khashab, *J. Am. Chem. Soc.* **2018**, *140*, 143; p) S. D. Jativa, N. Thapar, D. Broyles, E. Dikici, P. Daftarian, J. J. Jimenez, S. Daunert, S. K. Deo, *Mol. Pharmaceutics* **2019**, https://doi.org/10.1021/acs.molpharmaceut.8b01313.

[18] a) E. Afzal, S. Zakeri, P. Keyhanvar, M. Bagheri, P. Mahjoubi, M. Asadian, N. Omoomi, M. Dehqanian, M. Ghalandarlaki, T. Darvishmohammadi, F. Farjadian, M. S. Golvajoee, S. Afzal, M. Ghaffari, R. A. Cohan, A. Gravand, M. S. Ardestani, *Int. J. Nanomed.* **2013**, *8*, 2943; b) E. Bassi, S. Falzarano, M. Fabris, F. Gualandi, L. Merlini, G. Vattemi, D. Perrone, E. Marchesi, P. Sabatelli, K. Sparnacci,

M. Laus, P. Bonaldo, P. Rimessi, P. Braghetta, A. Ferlini, *J. Biomed. Biotechnol.* **2012**, *2012*, 897076; c) K. P. Bibee, Y. J. Cheng, J. K. Ching, J. N. Marsh, A. J. Li, R. M. Keeling, A. M. Connolly, P. T. Golumbek, J. W. Myerson, G. Hu, J. Chen, W. D. Shannon, G. M. Lanza, C. C. Weihl, S. A. Wickline, *FASEB J.* **2014**, *28*, 2047; d) P. K. Brown, A. T. Qureshi, A. N. Moll, D. J. Hayes, W. T. Monroe, *ACS Nano* **2013**, *7*, 2948; e) M. S. Falzarano, C. Passarelli, E. Bassi, M. Fabris, D. Perrone, P. Sabatelli, N. M. Maraldi, S. Dona, R. Selvatici, P. Bonaldo, K. Sparnacci, M. Laus, P. Braghetta, P. Rimessi, A. Ferlini, *Biomed. Res. Int.* **2013**, *2013*, 527418; f) Y. Kim, M. Tewari, J. D. Pajerowski, S. Cai, S. Sen, J. H. Williams, S. R. Sirsi, G. J. Lutz, D. E. Discher, *J. Controlled Release* **2009**, *134*, 132; g) N. Kinouchi, Y. Ohsawa, N. Ishimaru, H. Ohuchi, Y. Sunada, Y. Hayashi, Y. Tanimoto, K. Moriyama, S. Noji, *Gene Ther.* **2008**, *15*, 1126; h) T. Ochiya, Y. Takahama, S. Nagahara, Y. Sumita, A. Hisada, H. Itoh, Y. Nagai, M. Terada, *Nat. Med.* **1999**, *5*, 707; i) P. Rimessi, P. Sabatelli, M. Fabris, P. Braghetta, E. Bassi, P. Spitali, G. Vattemi, G. Tomelleri, L. Mari, D. Perrone, A. Medici, M. Neri, M. Bovolenta, E. Martoni, N. M. Maraldi, F. Gualandi, L. Merlini, M. Ballestri, L. Tondelli, K. Sparnacci, P. Bonaldo, A. Caputo, M. Laus, A. Ferlini, *Mol. Ther.* **2009**, *17*, 820; j) M. Wang, B. Wu, J. D. Tucker, L. E. Bollinger, P. Lu, Q. Lu, *Mol. Ther.–Nucleic Acids* **2016**, *5*, e341; k) J. H. Williams, R. C. Schray, S. R. Sirsi, G. J. Lutz, *BMC Biotechnol.* **2008**, *8*, 35; l) Y. Negishi, Y. Ishii, H. Shiono, S. Akiyama, S. Sekine, T. Kojima, S. Mayama, T. Kikuchi, N. Hamano, Y. Endo-Takahashi, R. Suzuki, K. Maruyama, Y. Aramaki, *Mol. Pharmaceutics* **2014**, *11*, 1053; m) M. Chiper, N. Tounsi, R. Kole, A. Kichler, G. Zuber, *J. Controlled Release* **2017**, *246*, 60; n) M. Costanzo, F. Vurro, B. Cisterna, F. Boschi, A. Marengo, E. Montanari, C. D. Meo, P. Matricardi, G. Berlier, B. Stella, S. Arpicco, M. Malatesta, *Nanomedicine* **2019**, *14*, 301; o) M. Wang, B. Wu, P. Lu, J. D. Tucker, S. Milazi, S. N. Shah, Q. L. Lu, *Gene Ther.* **2014**, *21*, 52; p) J. H. Williams, S. R. Sirsi, D. R. Latta, G. J. Lutz, *Mol. Ther.* **2006**, *14*, 88.

[19] G. Wenz, B. H. Han, A. Muller, *Chem. Rev.* **2006**, *106*, 782.

[20] Y. Ji, X. Liu, M. Huang, J. Jiang, Y. P. Liao, Q. Liu, C. H. Chang, H. Liao, J. Lu, X. Wang, M. J. Spencer, H. Meng, *Biomaterials* **2019**, *192*, 416.

[21] H. Yin, A. F. Saleh, C. Betts, P. Camelliti, Y. Seow, S. Ashraf, A. Arzumanov, S. Hammond, T. Merritt, M. J. Gait, M. J. Wood, *Mol. Ther.* **2011**, *19*, 1295.

[22] L. C. Ronn, M. Olsen, S. Ostergaard, V. Kiselyov, V. Berezin, M. T. Mortensen, M. H. Lerche, P. H. Jensen, V. Soroka, J. L. Saffell, P. Doherty, F. M. Poulsen, E. Bock, A. Holm, *Nat. Biotechnol.* **1999**, *17*, 1000.

[23] a) R. V. Benjaminsen, M. A. Mattebjerg, J. R. Henriksen, S. M. Moghimi, T. L. Andresen, *Mol. Ther.* **2013**, *21*, 149; b) M. Wojnilowicz, A. Glab, A. Bertucci, F. Caruso, F. Cavalieri, *ACS Nano* **2019**, *13*, 187; c) M. Xu, C. Y. Zhang, J. Wu, H. Zhou, R. Bai, Z. Shen, F. Deng, Y. Liu, J. Liu, *ACS Appl. Mater. Interfaces* **2019**, *11*, 5701, https://doi.org/10.1021/acsami.8b13059

[24] a) L. L. Ji, R. Fu, E. W. Mitchell, *J. Appl. Physiol.* **1992**, *73*, 1854; b) C. K. Sen, E. Marin, M. Kretzschmar, O. Hanninen, *J. Appl. Physiol.* **1992**, *73*, 1265; c) C. K. Sen, P. Rahkila, O. Hanninen, *Acta Physiol. Scand.* **1993**, *148*, 21; d) D. Montero, C. Tachibana, J. Rahr Winther, C. Appenzeller-Herzog, *Redox Biol.* **2013**, *1*, 508.

[25] M. R. Capecchi, *Cell* **1980**, *22*, 479.

[26] a) K. L. Capkovic, S. Stevenson, M. C. Johnson, J. J. Thelen, D. D. Cornelison, *Exp. Cell Res.* **2008**, *314*, 1553; b) A. Fidzianska, A. Kaminska, *Folia Neuropathol.* **1995**, *33*, 125; c) T. Snijders, J. P. Nederveen, B. R. McKay, S. Joanisse, L. B. Verdijk, L. J. van Loon, G. Parise, *Front. Physiol.* **2015**, *6*, 283.

[27] S. E. Moore, J. Thompson, V. Kirkness, J. G. Dickson, F. S. Walsh, *J. Cell Biol.* **1987**, *105*, 1377.

[28] a) J. A. Kulkarni, J. L. Myhre, S. Chen, Y. Y. C. Tam, A. Danescu, J. M. Richman, P. R. Cullis, *Nanomedicine* **2017**, *13*, 1377; b) L. M. Li, G. X. Ruan, M. Y. HuangFu, Z. L. Chen, H. N. Liu, L. X. Li, Y. L. Hu, M. Han, G. Davidson, P. A. Levkin, J. Q. Gao, *Int. J. Pharm.* **2015**, *488*, 1.

[29] D. Maddalo, E. Manchado, C. P. Concepcion, C. Bonetti, J. A. Vidigal, Y. C. Han, P. Ogrodowski, A. Crippa, N. Rekhtman, E. de Stanchina, S. W. Lowe, A. Ventura, *Nature* **2014**, *516*, 423.

[30] G. T. Zugates, D. G. Anderson, S. R. Little, I. E. Lawhorn, R. Langer, *J. Am. Chem. Soc.* **2006**, *128*, 12726.

[31] A. Yamashita, N. Yui, T. Ooya, A. Kano, A. Maruyama, H. Akita, K. Kogure, H. Harashima, *Nat. Protoc.* **2006**, *1*, 2861.

[32] T. Ooya, H. S. Choi, A. Yamashita, N. Yui, Y. Sugaya, A. Kano, A. Maruyama, H. Akita, R. Ito, K. Kogure, H. Harashima, *J. Am. Chem. Soc.* **2006**, *128*, 3852.

[33] C. Waldner, M. Roose, G. U. Ryffel, *BMC Dev. Biol.* **2009**, *9*, 37.

[34] T. Nomoto, S. Fukushima, M. Kumagai, K. Machitani, Arnida, Y. Matsumoto, M. Oba, K. Miyata, K. Osada, N. Nishiyama, K. Kataoka, *Nat. Commun.* **2014**, *5*, 3545.